Communications in Physics, Vol. 35, No. 4 (2025), pp. 315-324
DOI: https://doi.org/10.15625/0868-3166/23107

On Rydberg excitons in two-dimensional semiconductors

Hoang Ngoc Cam[1], **Nguyen Nhu Dat**[1], **Duong Thi Man**[1], **Pham Thi Bich Thao**[2], **and H. T. Nguyen-Truong**[3,†]

[1]*Institute of Physics, Vietnam Academy of Science and Technology, 10 Dao Tan, Giang Vo, Hanoi 11108, Vietnam*

[2]*College of Natural Sciences, Can Tho University, Can Tho City 900000, Vietnam*

[3]*Science and Technology Advanced Institute, Van Lang University, Ho Chi Minh City, Vietnam*

E-mail: †ntthieu@vlu.edu.vn

Received 1 July 2025; *Accepted for publication 16 September 2025*; *Published 9 December 2025*

Abstract. *We study Rydberg excitons in two-dimensional transition-metal dichalcogenide semiconductors, using the Rytova-Keldysh potential to account for nonlocal dielectric screening effects. We determine exciton binding energies in monolayer WSe_2 and WS_2 by the variational method. We perform calculations for different dielectric environments (isolation, hBN encapsulation, and SiO_2 substrate support) to investigate the influences of the surrounding dielectric environment. Our theoretical results agree reasonably with experimental measurements and previous numerical calculations. The study shows a strong dependence of exciton binding energy and spatial extent on both the principal and angular quantum numbers, as well as on the surrounding dielectric environment.*

Keywords: Rydberg excitons, 2D semiconductors.

Classification numbers: 71.35.-y; 71.35.Cc; 78.67.-n.

1. Introduction

Over the past decade, monolayer transition metal dichalcogenide (TMD) semiconductors with direct bandgaps in the near-infrared to visible spectral range have emerged as promising materials for next-generation photonic and optoelectronic devices such as light-emitting diodes [1–3], photodetectors [4], and lasers [5, 6]. The reduced dimensionality and dielectric screening in these two-dimensional (2D) materials significantly enhance Coulomb interactions, resulting in tightly bound excitons (electron-hole pairs) with large binding energies. These excitons are stable even at room temperature and dominate the optical properties of monolayer TMDs [7–9]. Of particular interest are the highly excited excitonic states, known as Rydberg excitons, which exhibit large spatial extents and dipole moments. The strong long-range dipole-dipole interactions make Rydberg excitons highly sensitive to external perturbations and hence attractive for quantum technologies [10–13].

Understanding Rydberg exciton properties, particularly under the influence of the surrounding dielectric environment, is necessary for the development of excitonic devices. Here, we determine the binding energy of Rydberg excitons in monolayer WSe_2 and WS_2 using the variational method. This method is often used to provide a comparison with numerical or experimental results. While many variational studies are interested in the groundstate exciton [14–21], we are interested in Rydberg excitons (i.e. excited excitonic states) of both zero and finite angular momentum quantum numbers. Our variational calculations can be applied to 2D isotropic semiconductors. The variational method can also be applied to 2D anisotropic semiconductors [22–25]. However, the direction-dependent dispersion of band edges, which is indispensable in anisotropic studies, is beyond the scope of the present work. In this work we assume the dispersion of band edges to be direction-independent and focus on isotropic materials. We describe electron-hole interactions using the Rytova-Keldysh potential [26, 27], which is more accurate than the Coulomb potential in taking into account nonlocal dielectric screening effects characteristic of 2D materials. We perform calculations for different dielectric environments (isolation, hBN encapsulation, and SiO_2 substrate support) to investigate the influences of the surrounding dielectric environment. We compare with experimental data [10] and previous numerical solutions of the 2D Schrödinger equation [28] to validate the obtained results.

In the past decade, some expressions for the exciton binding energy in 2D semiconductors have been introduced [28–31], including semi-empirical formulas [32]. Using the variational method, our purpose here is to derive an exciton energy function (its minimum is an upper bound to the exciton energy) rather than an analytical expression for the exciton binding energy. Furthermore, we are interested in Rydberg excitons of both zero and non-zero angular momentum quantum numbers, while the previous works mainly focus on excitons of the zero angular momentum quantum number.

2. Theory

In the effective-mass approximation, the 2D Schrödinger equation for Wannier–Mott excitons reads (in Hartree atomic units)

$$\left(-\frac{1}{2\mu}\nabla_{2D}^2 + V(r)\right)\psi(\boldsymbol{r}) = E\,\psi(\boldsymbol{r}), \tag{1}$$

where μ is the exciton reduced mass, ∇_{2D}^2 is the 2D Laplacian in polar coordinates $\boldsymbol{r} = (r, \varphi)$,

$$\nabla_{2D}^2 = \frac{1}{r}\frac{\partial}{\partial r}\left(r\frac{\partial}{\partial r}\right) + \frac{1}{r^2}\frac{\partial^2}{\partial \varphi^2}, \tag{2}$$

and $V(r)$ is the Rytova-Keldysh potential [26, 27]

$$V(r) = -\frac{\pi}{2r_0}\left[\mathbf{H}_0\left(\frac{\kappa r}{r_0}\right) - Y_0\left(\frac{\kappa r}{r_0}\right)\right], \tag{3}$$

where $\mathbf{H}_0$ is the Struve function, Y_0 is the Bessel function of the second kind, κ is the average environmental dielectric constant, r is the electron-hole distance, and r_0 is the screening length.

Assuming cylindrical symmetry, the envelope function $\psi(\boldsymbol{r})$ can be expressed as

$$\psi_{nm}(\boldsymbol{r}) = \psi_{nm}(r, \varphi) = \frac{e^{im\varphi}}{\sqrt{2\pi}} R_{nm}(r), \tag{4}$$

where (n,m) is the (principal, angular momentum) quantum number, and the radial function $R_{nm}(r)$ is the solution of the radial equation

$$-\frac{1}{2\mu}\left[\frac{1}{r}\frac{\mathrm{d}}{\mathrm{d}r}\left(r\frac{\mathrm{d}}{\mathrm{d}r}\right)-\frac{m^2}{r^2}\right]R_{nm}(r)+V(r)R_{nm}(r)=E_{nm}R_{nm}(r). \tag{5}$$

We find $R_{nm}(r)$ in the form of the widely-known 2D hydrogenic trial function [33–37]

$$R_{nm}(r)=C_{nm}\frac{2}{a_{nm}}\left(\frac{2r}{a_{nm}}\right)^{|m|}\exp\left(-\frac{r}{a_{nm}}\right)L^{2|m|}_{n-|m|-1}\left(\frac{2r}{a_{nm}}\right), \tag{6}$$

where L denotes the generalized Laguerre polynomial, a_{nm} is a variational parameter, and C_{nm} is the normalization constant. From the normalization condition

$$1=\langle\psi^*_{nm}|\psi_{nm}\rangle=\int\psi^*_{nm}(\boldsymbol{r})\psi_{nm}(\boldsymbol{r})\mathrm{d}\boldsymbol{r}=\int_0^{2\pi}\int_0^{\infty}\psi^*_{nm}(r,\varphi)\psi_{nm}(r,\varphi)r\mathrm{d}r\mathrm{d}\varphi=\int_0^{\infty}R^2_{nm}(r)r\mathrm{d}r, \tag{7}$$

we have

$$\langle R_{nm}|r|R_{nm}\rangle=C^2_{nm}(2n-1)\frac{(n+|m|-1)!}{(n-|m|-1)!}=1, \tag{8}$$

i.e.

$$C_{nm}=\frac{1}{\sqrt{2n-1}}\sqrt{\frac{(n-|m|-1)!}{(n+|m|-1)!}}. \tag{9}$$

Applying the normalization condition (7) to the radial equation (5), we obtain

$$-\frac{1}{2\mu}\left\langle R_{nm}\middle|r\left[\frac{1}{r}\frac{\mathrm{d}}{\mathrm{d}r}\left(r\frac{\mathrm{d}}{\mathrm{d}r}\right)-\frac{m^2}{r^2}\right]\middle|R_{nm}\right\rangle+\langle R_{nm}|rV(r)|R_{nm}\rangle=E_{nm}\langle R_{nm}|r|R_{nm}\rangle. \tag{10}$$

Since

$$\left\langle R_{nm}\middle|r\left[\frac{1}{r}\frac{\mathrm{d}}{\mathrm{d}r}\left(r\frac{\mathrm{d}}{\mathrm{d}r}\right)-\frac{m^2}{r^2}\right]\middle|R_{nm}\right\rangle=-\frac{1}{a^2_{nm}}, \tag{11}$$

we are able to express E_{nm} as a function of the variational parameter a_{nm} as follows:

$$E_{nm}(a_{nm})=\frac{1}{2\mu a^2_{nm}}-\frac{\pi}{2r_0}C^2_{nm}D_{nm}\left(\frac{2r_0}{a_{nm}\kappa}\right), \tag{12}$$

where

$$D_{nm}(b)=b\int_0^{\infty}\left[\mathbf{H}_0(x)-Y_0(x)\right](bx)^{2|m|+1}e^{-bx}\left[L^{2|m|}_{n-|m|-1}(bx)\right]^2\mathrm{d}x. \tag{13}$$

Minimizing the variational energy function $E_{nm}(a_{nm})$, i.e. solving $\mathrm{d}E_{nm}(a_{nm})/\mathrm{d}a_{nm}=0$, we find the lowest variational energy $E^{\min}_{nm}$ at each state (n,m), which is an upper bound of the exciton energy. Because the exact value of the exciton energy is unknown, $E^{\min}_{nm}$ is often assumed to be the exciton energy (its absolute value is the exciton binding energy) of the state (n,m).

3. Results and discussion

Figure 1(a) displays the variational energy function (12) of excitons in hBN-encapsulated monolayer WSe_2 ($\mu = 0.2$ and $\kappa = 4.5$ [38], $r_0 = 4.0$ nm). The red circles indicate the lowest variational energy at each state, which is an upper bound of the corresponding exciton energy (its exact value is unknown). The upper bound is considered as the exciton energy, the absolute value of which is the exciton binding energy. The radial function (6) results in the exciton energy function (12) consisting of two opposite terms: the first term in the right hand side of Eq. (12) is positive and decreases with increasing the variational parameter a_{nm} (see Fig. 1(b)), while the second one is negative and increases as a_{nm} increases (see Fig. 1(c)). Summing these two terms yields the exciton energy function with a behavior similar to a two-body interaction potential such as the Lennard-Jones potential with only one minimum. Note that due to the exponential term e^{-bx} in the integral (13), the main contribution to the integral is located at small bx, and hence the complicated behavior of the generalized Laguerre polynomial over the range $(0,\infty)$ has almost no influence on the monotonic behavior of D_{nm}. Therefore, the exciton energy function (12) has only one minimum at each state as indicated by red circles in Fig. 1(a). Table 1 lists the exciton binding energy (the absolute value of the exciton energy) alongside experimental results [10] for excitons in hBN-encapsulated monolayer WSe_2. The deviations between the theoretical and experimental values are less than 1 meV, showing the reliability of the present variational calculations.

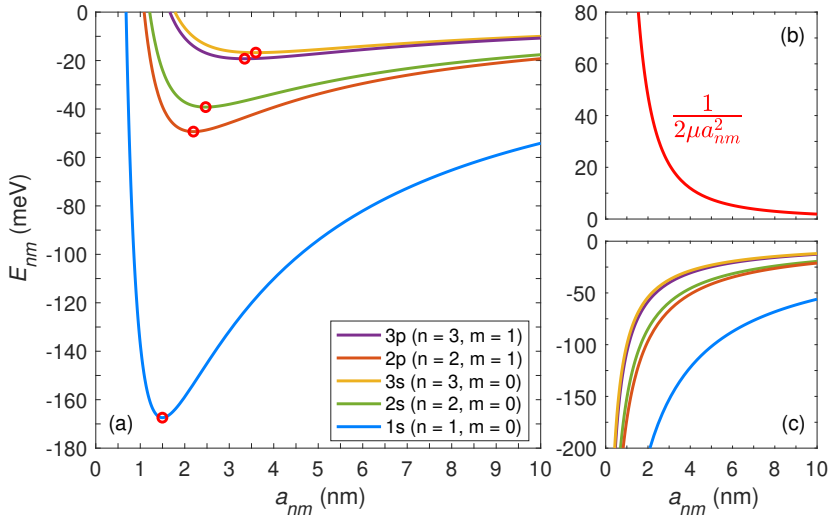

Fig. 1. (Color online) Excitons in hBN-encapsulated monolayer WSe_2: (a) The variational energy function (12), the red circles indicate the minima of this function at different states; (b) The first term in the right hand side of Eq. (12); (c) The second term in the right hand side of Eq. (12).

Figure 2 shows the ns-exciton binding energy for isolated monolayer WS_2 ($\mu = 0.17$, $r_0 = 3.4$ nm, and $\kappa = 1.0$). The present variational result (red circles) agree quantitatively with the previous numerical solution of the 2D Schrodinger equation [28] (blue squares). The inset of Fig. 2 displays the radial functions.

Table 1. The variational and experimental results for excitons in hBN-encapsulated monolayer WSe_2.

Exciton	Variational results		Experimental results [10]
	a_{nm} (nm)	$-E_{nm}^{\min}$ (meV)	Binding energy (meV)
$1s$	1.5	167.4	168.6
$2s$	2.5	39.2	40.0
$3s$	3.6	16.7	17.4
$4s$	4.8	9.2	9.7
$5s$	5.9	5.8	6.1
$6s$	7.1	4.0	4.2
$7s$	8.3	2.9	3.1
$8s$	9.5	2.2	2.4
$9s$	10.7	1.7	1.9
$10s$	11.9	1.4	1.5
$11s$	13.1	1.1	1.2
$2p$	2.2	49.3	
$3p$	3.3	19.2	
$4p$	4.5	10.1	
$5p$	5.7	6.2	

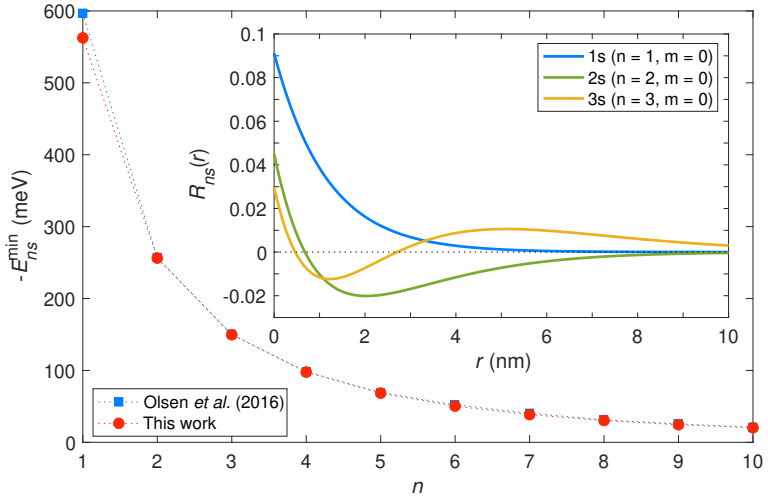

Fig. 2. (Color online) The binding energy of excitons in isolated monolayer WS_2. The inset displays the radial functions.

To investigate the influence of the surrounding dielectric environment, we perform variational calculations for monolayer WS_2 with and without substrate effects. Table 2 lists variational results for monolayer WS_2 on SiO_2 substrate (the average environmental dielectric constant $\kappa = 2.4$ corresponds to the substrate dielectric constant $\varepsilon_{SiO_2} = 3.8$ [18]) and for isolated monolayer WS_2 ($\kappa = 1$). Compared to the isolated monolayer WS_2, the dielectric screening within the

monolayer WS_2 on SiO_2 substrate is enhanced due to substrate effects, the electron-hole interaction strength (and hence the exciton binding energy) is therefore reduced.

Table 2. The variational results with and without substrate effects for excitons in monolayer WS_2.

Exciton	Isolated monolayer WS_2 $\kappa = 1$		Monolayer WS_2 on SiO_2 substrate $\kappa = 2.4$	
	a_{nm} (nm)	$-E_{nm}^{\min}$ (meV)	a_{nm} (nm)	$-E_{nm}^{\min}$ (meV)
1s	1.2	562.5	1.3	303.1
2s	1.4	256.2	1.9	92.6
3s	1.6	149.7	2.5	43.4
4s	1.8	97.7	3.2	24.8
5s	2.1	68.4	4.0	16.0
6s	2.4	50.3	4.7	11.1
7s	2.7	38.5	5.4	8.2
8s	3.0	30.3	6.2	6.3
9s	3.3	24.5	6.9	5.0
10s	3.6	20.2	7.7	4.0
2p	1.3	298.9	1.7	115.0
3p	1.5	163.6	2.4	49.5
4p	1.8	103.9	3.1	27.3
5p	2.1	71.7	3.8	17.2

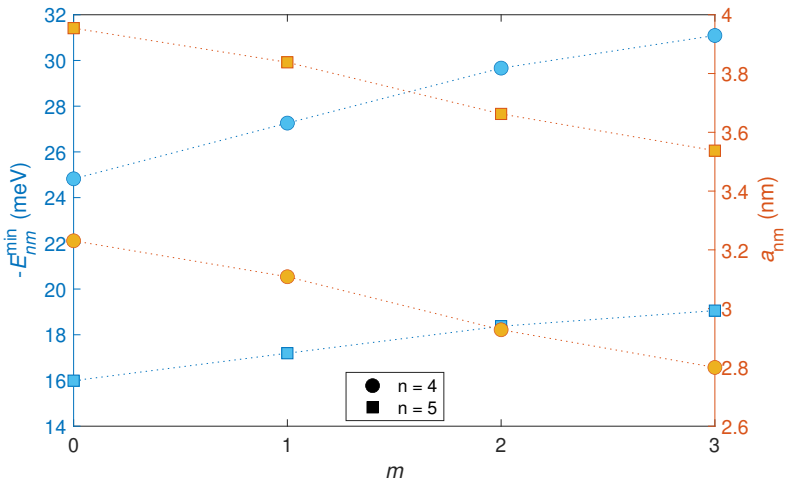

Fig. 3. (Color online) Monolayer WS_2 on SiO_2 substrate: the exciton binding energy (left) and the corresponding variational parameter (right) as functions of the angular quantum number for fixed principal quantum numbers.

We also investigate the dependence of the exciton binding energy $-E_{nm}^{\min}$ (and the corresponding variational parameter a_{nm}) on the angular quantum number m at fixed principal quantum

numbers n. Fig. 3 displays $-E_{nm}^{\min}$ and a_{nm} as functions of m at $n=4$ and $n=5$ for monolayer WS_2 on SiO_2 substrate. In general, the exciton binding energy is inversely proportional to the principal quantum number but is directly proportional to the angular momentum quantum number. In monolayer TMDs, an exciton can be optically bright or dark depending on its angular momentum quantum number. For instance, s- and d-state excitons (corresponding to $m=0$ and $m=2$, respectively) are optically bright, while p-state excitons ($m=1$) are optically dark [39]. These excitons are located at the K and K' valleys of the first Brillouin zone, and are excited by σ^+ and σ^- circularly polarized light, respectively [39]. They obey valley-dependent optical selection rules, suggesting the possibility of valley optoelectronic devices [40, 41]. The electrically switchable chiral light-emitting transistor based on monolayer WSe_2 is an example [42].

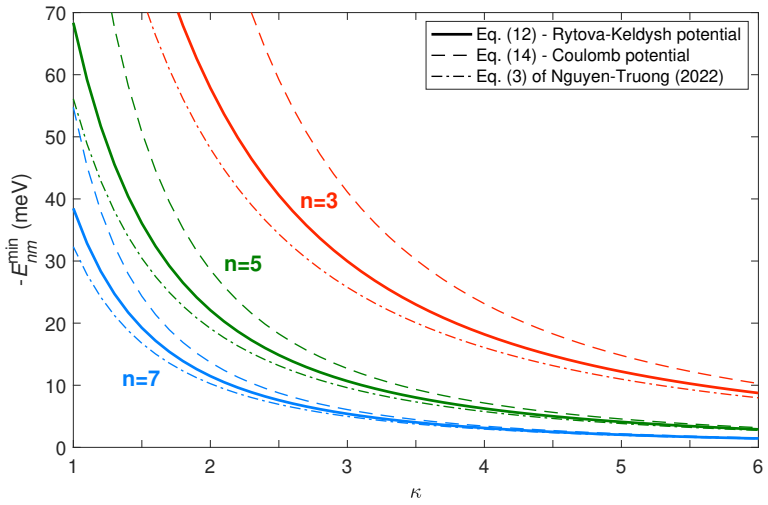

Fig. 4. (Color online) Monolayer WS_2: the exciton binding energy as a function of the average environmental dielectric constant. Solid line represents the minimum of the energy function (12) for Rytova-Keldysh-excitons, dashed line represents the Coulomb-exciton energy (14), and dash-dotted line represents the exciton energy given by Eq. (3) in Ref. 31.

Finally, we investigate the dependence of the exciton binding energy $-E_{nm}^{\min}$ on the average environmental dielectric constant κ. Figure 4 plots $-E_{nm}^{\min}$ as a function of κ for Rydberg excitons in monolayer WS_2. Increasing the average environmental dielectric enhances the dielectric screening, and reduces the electron-hole interaction strength, hence decreases the exciton binding energy. In addition, the electron-hole distance is directly proportional to the average environmental dielectric. At large electron-hole distances, the Rytova-Keldysh potential returns to the Coulomb potential, then the Schrödinger equation (1) can be solved analytically to derive exactly the exciton energy

$$E_{nm}^{*} = -\frac{\mu}{2\kappa^2\left(n+|m|-\frac{1}{2}\right)^2}. \tag{14}$$

In Fig. 4, the variational binding energy $-E_{nm}^{\min}$ approaches the Coulomb-exciton binding energy $-E_{nm}^{*}$ with increasing κ and n, showing again the reliability of the present calculations. The s-state excitons exhibit a hydrogenic behavior for $n \gg 1$. Nonetheless, due to influences of the

surrounding dielectric environment, the hydrogenic behavior of s-state excitons depends not only on the principal quantum number (n) but also on the average environmental dielectric constant (κ). Fig. 4 shows that 7s-excitons (blue lines) exhibit the hydrogenic behavior at $\kappa > 4$, while 5s-excitons (green lines) only exhibit the hydrogenic behavior at $\kappa > 5$ (or even higher). The difference between the Coulomb-excitons (dashed lines) and Rytova-Keldysh-excitons (solid lines) increases with decreasing κ and n.

Figure 4 also includes the exciton binding energy predicted by the expression (3) in Ref. 31. This expression was derived by solving the 2D Schrödinger equation (1) for Wannier–Mott excitons using a logarithm potential to approximate the Rytova-Keldysh potential (3). With increasing κ and n all curves are consistent with each other, in which the variational results (solid line) approach faster to the predicted value (dash-dotted line) than the Coulomb-exciton binding energy (dashed line). This is because the present variational energy function and the previous expression for the exciton binding energy [31] were based on the the Rytova-Keldysh potential (3) but not the Coulomb potential. The agreement confirms the reliability of these variational calculations.

Because the effect of the dielectric environment is of particular interest, it is necessary to evaluate the reliability of the obtained variational energy. As listed in Table 2, the variational binding energy of the ground-state exciton in a monolayer WS_2 on SiO_2 substrate is $E_b^{var} = 0.303$ eV, while the experimental value from reflectance contrast measurements is $E_b^{expt} = 0.32 \pm 0.04$ eV [43]. Thus, the deviation $(E_b^{expt} - E_b^{var})/E_b^{expt}$ is 5.31 %. Here we use $\mu = 0.17$ [44], $r_0 = 3.4$ nm [45], and $\kappa = 2.4$ (corresponding to $\varepsilon_{SiO_2} = 3.8$ [18]). Note that the value of a parameter for the same material in different studies could be different, such as the exciton reduced mass in a monolayer WS_2 (0.15 [46], 0.16 [43], 0.17 [44], and 0.19 [28]). In addition, the measured exciton reduced mass has been found to be heavier than that calculated using the density functional theory [45]. The reason for this phenomenon remains unclear. In general, the variational method provides an upper bound to the exciton energy, i.e. a lower bound to the exciton binding energy ($E_b^{var} < E_b^{expt}$). The reliability of the variational energy strongly depends on the choice of the trial function. Although this method only provides approximate solutions, it is still a useful tool due to its simplicity and effectivity.

The above comparisons show the suitability of the trial function (6) and the validity of the energy function (12), two important factors in a variational study. Apart from the well-known variational method, the exciton problem can also be studied using highly precise numerical methods such as the finite difference method [38], the Bessel discrete variable representation [10], or the Feranchuk-Komarov operator method [47].

4. Conclusions

In this work we have determined Rydberg exciton energies in monolayers WS_2 and WSe_2 by the variational method. We have used the Rytova-Keldysh potential to describe the electron-hole interaction, taking into account the environmental dielectric screening. Comparing with the previous experimental and numerical results, we have shown the reliability of the present variational calculations. We have also shown the influence of the surrounding dielectric environment on the Rydberg exciton energy.

Acknowledgements

This research is funded by Vietnam National Foundation for Science and Technology Development (NAFOSTED) under grant number 103.01-2023.114.

Conflict of interest

The authors have no conflict of interest.

References

[1] B. W. H. Baugher, H. O. H. Churchill, Y. Yang and P. Jarillo-Herrero, *Optoelectronic devices based on electrically tunable p–n diodes in a monolayer dichalcogenide*, Nat. Nanotechnol. **9** (2014) 262.
[2] A. Pospischil, M. M. Furchi and T. Mueller, *Solar-energy conversion and light emission in an atomic monolayer p–n diode*, Nat. Nanotechnol. **9** (2014) 257.
[3] J. S. Ross, P. Klement, A. M. Jones, N. J. Ghimire, J. Yan, D. G. Mandrus *et al.*, *Electrically tunable excitonic light-emitting diodes based on monolayer WSe_2 p–n junctions*, Nat. Nanotechnol. **9** (2014) 268.
[4] H. Wang, C. Zhang, W. Chan, S. Tiwari and F. Rana, *Ultrafast response of monolayer molybdenum disulfide photodetectors*, Nat. Commun. **6** (2015) 8831.
[5] S. Wu, S. Buckley, J. R. Schaibley, L. Feng, J. Yan, D. G. Mandrus *et al.*, *Monolayer semiconductor nanocavity lasers with ultralow thresholds*, Nature **520** (2015) 69.
[6] Y. Ye, Z. J. Wong, X. Lu, X. Ni, H. Zhu, X. Chen *et al.*, *Monolayer excitonic laser*, Nat. Photonics **9** (2015) 733.
[7] D. Y. Qiu, F. H. da Jornada and S. G. Louie, *Optical spectrum of mos_2: Many-body effects and diversity of exciton states*, Phys. Rev. Lett. **111** (2013) 216805.
[8] K. He, N. Kumar, L. Zhao, Z. Wang, K. F. Mak, H. Zhao *et al.*, *Tightly bound excitons in monolayer* wse_2, Phys. Rev. Lett. **113** (2014) 026803.
[9] M. M. Ugeda, A. J. Bradley, S.-F. Shi, F. H. da Jornada, Y. Zhang, D. Y. Qiu *et al.*, *Giant bandgap renormalization and excitonic effects in a monolayer transition metal dichalcogenide semiconductor*, Nat. Mater. **13** (2014) 1091.
[10] T. Wang, Z. Li, Y. Li, Z. Lu, S. Miao, Z. Lian *et al.*, *Giant valley-polarized rydberg excitons in monolayer wse_2 revealed by magneto-photocurrent spectroscopy*, Nano Lett. **20** (2020) 7635.
[11] A. Popert, Y. Shimazaki, M. Kroner, K. Watanabe, T. Taniguchi, A. Imamoğlu *et al.*, *Optical sensing of fractional quantum hall effect in graphene*, Nano Lett. **22** (2022) 7363.
[12] Q. Hu, Z. Zhan, H. Cui, Y. Zhang, F. Jin, X. Zhao *et al.*, *Observation of rydberg moiré excitons*, Science **380** (2023) 1367.
[13] Z. Lian, Y.-M. Li, L. Yan, L. Ma, D. Chen, T. Taniguchi *et al.*, *Stark effects of rydberg excitons in a monolayer WSe_2 p–n junction*, Nano Lett. **24** (2024) 4843.
[14] T. C. Berkelbach, M. S. Hybertsen and D. R. Reichman, *Theory of neutral and charged excitons in monolayer transition metal dichalcogenides*, Phys. Rev. B **88** (2013) 045318.
[15] C. Zhang, H. Wang, W. Chan, C. Manolatou and F. Rana, *Absorption of light by excitons and trions in monolayers of metal dichalcogenide mos_2: Experiments and theory*, Phys. Rev. B **89** (2014) 205436.
[16] Y. You, X.-X. Zhang, T. C. Berkelbach, M. S. Hybertsen, D. R. Reichman and T. F. Heinz, *Observation of biexcitons in monolayer WSe_2*, Nat. Phys. **11** (2015) 477.
[17] E. Courtade, M. Semina, M. Manca, M. M. Glazov, C. Robert, F. Cadiz *et al.*, *Charged excitons in monolayer* wse_2*: Experiment and theory*, Phys. Rev. B **96** (2017) 085302.
[18] M. Van der Donck, M. Zarenia and F. M. Peeters, *Excitons, trions, and biexcitons in transition-metal dichalcogenides: Magnetic-field dependence*, Phys. Rev. B **97** (2018) 195408.
[19] R. P. A. Emmanuele, M. Sich, O. Kyriienko, V. Shahnazaryan, F. Withers, A. Catanzaro *et al.*, *Highly nonlinear trion-polaritons in a monolayer semiconductor*, Nat. Commun. **11** (2020) 3589.
[20] H. N. Cam, N. T. Phuc and V. A. Osipov, *Symmetry-dependent exciton-exciton interaction and intervalley biexciton in monolayer transition metal dichalcogenides*, npj 2D Mater. Appl. **6** (2022) 22.
[21] I. L. C. Lima, M. V. Milošević, F. M. Peeters and A. Chaves, *Tuning of exciton type by environmental screening*, Phys. Rev. B **108** (2023) 115303.

[22] A. Castellanos-Gomez, L. Vicarelli, E. Prada, J. O. Island, K. Narasimha-Acharya, S. I. Blanter *et al.*, *Isolation and characterization of few-layer black phosphorus*, 2D Mater. **1** (2014) 025001.
[23] E. Prada, J. V. Alvarez, K. L. Narasimha-Acharya, F. J. Bailen and J. J. Palacios, *Effective-mass theory for the anisotropic exciton in two-dimensional crystals: Application to phosphorene*, Phys. Rev. B **91** (2015) 245421.
[24] L. Xu, M. Yang, S. J. Wang and Y. P. Feng, *Electronic and optical properties of the monolayer group-iv monochalcogenides mx (m = ge, sn; x = s, se, te)*, Phys. Rev. B **95** (2017) 235434.
[25] J. N. S. Gomes, C. Trallero-Giner and M. I. Vasilevskiy, *Variational calculation of the lowest exciton states in phosphorene and transition metal dichalcogenides*, J. Phys.: Condens. Matter **34** (2022) 045702.
[26] N. S. Rytova, *The screened potential of a point charge in a thin film*, Moscow Univ. Phys. Bull. **22** (1967) 18.
[27] L. V. Keldysh, *Coulomb interaction in thin semiconductor and semimetal films*, JETP Lett. **29** (1979) 658.
[28] T. Olsen, S. Latini, F. Rasmussen and K. S. Thygesen, *Simple screened hydrogen model of excitons in two-dimensional materials*, Phys. Rev. Lett. **116** (2016) 056401.
[29] M. R. Molas, A. O. Slobodeniuk, K. Nogajewski, M. Bartos, L. Bala, A. Babiński *et al.*, *Energy spectrum of two-dimensional excitons in a nonuniform dielectric medium*, Phys. Rev. Lett. **123** (2019) 136801.
[30] A. C. Riis-Jensen, M. N. Gjerding, S. Russo and K. S. Thygesen, *Anomalous exciton rydberg series in two-dimensional semiconductors on high-kappa dielectric substrates*, Phys. Rev. B **102** (2020) 201402.
[31] H. T. Nguyen-Truong, *Exciton binding energy and screening length in two-dimensional semiconductors*, Phys. Rev. B **105** (2022) L201407.
[32] H. T. Dinh, N.-H. Phan, D.-N. Ly, D.-N. Le, N.-T. D. Hoang, N.-Q. Nguyen *et al.*, *Analytical expression for exciton energies in monolayer transition metal dichalcogenides*, Phys. Rev. B **111** (2025) 035443.
[33] M. Shinada and S. Sugano, *Interband optical transitions in extremely anisotropic semiconductors. i. bound and unbound exciton absorption*, J. Phys. Soc. Jpn. **21** (1966) 1936.
[34] W. Edelstein, H. N. Spector and R. Marasas, *Two-dimensional excitons in magnetic fields*, Phys. Rev. B **39** (1989) 7697.
[35] X. L. Yang, S. H. Guo, F. T. Chan, K. W. Wong and W. Y. Ching, *Analytic solution of a two-dimensional hydrogen atom. i. nonrelativistic theory*, Phys. Rev. A **43** (1991) 1186.
[36] D. G. W. Parfitt and M. E. Portnoi, *The two-dimensional hydrogen atom revisited*, J. Math. Phys. **43** (2002) 4681.
[37] H. Haug and S. W. Koch, *Quantum Theory of the Optical and Electronic Properties of Semiconductors*. World Scientific, Singapore, 2004.
[38] A. V. Stier *et al.*, *Magnetooptics of exciton rydberg states in a monolayer semiconductor*, Phys. Rev. Lett. **120** (2018) 057405.
[39] K. F. Mak, D. Xiao and J. Shan, *Light–valley interactions in 2d semiconductors*, Nat. Photonics **12** (2018) 451.
[40] K. F. Mak, K. He, J. Shan and T. F. Heinz, *Control of valley polarization in monolayer mos_2 by optical helicity*, Nat. Nanotechnol. **7** (2012) 494.
[41] J. R. Schaibley, H. Yu, G. Clark, P. Rivera, J. S. Ross, K. L. Seyler *et al.*, *Valleytronics in 2d materials*, Nat. Rev. Mater. **1** (2016) 16055.
[42] Y. J. Zhang, T. Oka, R. Suzuki, J. T. Ye and Y. Iwasa, *Electrically switchable chiral light-emitting transistor*, Science **344** (2014) 725.
[43] A. Chernikov, T. C. Berkelbach, H. M. Hill, A. Rigosi, Y. Li, B. Aslan *et al.*, *Exciton binding energy and nonhydrogenic rydberg series in monolayer* ws_2, Phys. Rev. Lett. **113** (2014) 076802.
[44] T. Handa, M. Holbrook, N. Olsen, L. N. Holtzman, L. Huber, H. I. Wang *et al.*, *Spontaneous exciton dissociation in transition metal dichalcogenide monolayers*, Sci. Adv. **10** (2024) eadj4060.
[45] M. Goryca, J. Li, A. V. Stier, T. Taniguchi, K. Watanabe, E. Courtade *et al.*, *Revealing exciton masses and dielectric properties of monolayer semiconductors with high magnetic fields*, Nat. Commun. **10** (2019) 4172.
[46] J. Zipfel, J. Holler, A. A. Mitioglu, M. V. Ballottin, P. Nagler, A. V. Stier *et al.*, *Spatial extent of the excited exciton states in* ws_2 *monolayers from diamagnetic shifts*, Phys. Rev. B **98** (2018) 075438.
[47] D.-N. Ly, D.-N. Le, D.-A. P. Nguyen, N.-T. D. Hoang, N.-H. Phan, H.-M. L. Nguyen *et al.*, *Retrieval of material properties of monolayer transition metal dichalcogenides from magnetoexciton energy spectra*, Phys. Rev. B **107** (2023) 205304.